Open access Original scientific paper

https://doi.org/10.5552/crojfe.2025.2434

Traction Assistance of a Forwarder in Flat Terrain: Effects on Wheel Slip and Soil Disturbance

Lorenz Breinig, Bastian Hinte, Marian Schönauer, Stephan Hoffmann, Henrik Brokmeier, Dirk Jaeger

Abstract

Traction assistance of forest machines via traction aid winches has gained widespread application in steep-terrain forest operations as it can mitigate soil disturbance by reducing wheel or track slip of the assisted machine. Since slip affects machine operations in flat terrain as well, especially on fine-grained and moist soils, the effectiveness of traction assistance under such conditions was evaluated. At a forest site, a forwarder with a total mass of 28.6 t was driven over two plots in 15 passes. The machine travelled unassisted over one plot, while on the second plot traction assistance was manually adjusted to keep slip close to 0%. Wheel slip and winch tractive force were recorded during each pass, and rut depth was measured after each pass. Soil density was measured pre-impact and at three times after different traffic increments. Although the mean wheel slip was low even during unassisted travel, traction assistance was found to cause a significant reduction. While both a decrease in rut depth and soil compaction were observed with traction assistance, only the latter was significant after three machine passes. A potential influence of inhomogeneous soil reinforcement due to roots suggests repeating the experiment on a more homogenous soil.

Keywords: forest operations, timber harvesting, tethered logging, winch-assist, machine–soil interaction, soil compaction, wheel ruts, environmental impact

1. Introduction

Mechanized timber harvesting using ground-based forest machines such as harvesters and forwarders in cut-to-length systems, or feller-bunchers, skidders and processors in full-tree systems, is an indispensable element of forest management due to the high level of productivity and work safety it provides (Labelle et al. 2022). However, physical disturbance of forest soils, i.e. soil compaction and rut formation, caused by high machine masses resulting in high dynamic ground pressures and shear forces as well as by wheel or track slip when travelling on adverse ground conditions is a well-documented problem from both operational and ecological perspectives often entailed by utilizing ground-based forest machines (Froehlich 1978, Wästerlund 1989, McNabb et al. 2001, Ampoorter et al. 2007, Horn et al. 2007, Labelle and Jaeger 2011, Cambi et al. 2015, Labelle et al. 2022).

Two separate but interrelated characteristics of soil disturbance are commonly described: soil compaction and rut formation (Cambi et al. 2015). The susceptibility of a soil to deformation is determined by its texture (particle size distribution) and share of coarse fraction, moisture content, initial bulk density (pre-compaction state), organic matter content, aggregation of primary particles, particle roundness and even certain chemical properties (Amelung et al. 2018). Texture and moisture content are commonly assumed to be the prevailing factors (Wästerlund 1989, McNabb et al. 2001, Allman et al. 2017, Naghdi et al. 2020, Labelle et al. 2022). In forest soils, soil stability is also influenced to a large extent by the reinforcing effect of roots (Wästerlund 1989). Technical approaches to mitigate soil disturbance due to forest machine traffic comprise the use of wide tires (Haas et al. 2016), bogie tracks (Bygdén et al. 2003, Labelle and Jaeger 2019, Ala-Ilomäki et al. 2021), reduced tire inflation pressure (Eliasson 2005),

additional wheels (Ala-Ilomäki et al. 2011, Starke et al. 2020) or rubber tracks with suspension systems (Gelin and Björheden 2021). Among operational countermeasures to soil deformation, armoring the ground with treetops and limbs, the so-called brush mats, is common practice (Eliasson and Wästerlund 2007, Labelle and Jaeger 2012).

Providing traction assistance to ground-based forest machines by the tractive force of a winch, also referred to as cable-assistance, tethering or winch-assist, is used to increase their gradeability while preventing excessive wheel or track slip and thus to extend their application to operations on steep slopes where inclination is greater than 30% and may even exceed 50% (Visser and Stampfer 2015, Holzleitner et al. 2018, Cavalli and Amishev 2019). This technology was first described in a feasibility study from 1978 (McKenzie and Richardson, 1978) and it has gained widespread application with wheeled and tracked machines in both cut-to-length and full-tree systems during the last two decades (Mologni et al. 2018, Holzfeind et al. 2020). A recent standard, ISO 19472-2:2022 (ISO 2022), classifies winches for traction assistance into two categories: Traction aid winches only provide additional tractive effort for the purpose of slip reduction while the assisted machine must still be stable against tipping over and capable to prevent sliding on its own. Climbing support winches, in contrast, are designed to fully secure the stability of the assisted machine on the slope and must thus be dimensioned accordingly. Only the former type is currently used in Germany, and therefore operational guidelines by state forest authorities usually restrict ground-based harvesting to sites with less than 45% inclination.

Recent literature suggests that traction assistance is effective in mitigating soil disturbance during ground-based operations in sloped terrain (Holzfeind et al. 2020). Estimating the effects of traction assistance in a theoretical approach, Sessions et al. (2017) calculated peak ground pressures and maximum operational slope angles for a tracked machine when applying different levels of tractive force through a tether line. They reported a marked reduction in peak ground pressures with increasing tractive force assuming a linear contact pressure distribution under the tracks and a track slip of 15%. Garren et al. (2019) assessed soil bulk density and rut depth after tethered forwarding on slopes of varying inclination in Brazil and attributed an effective reduction of soil compaction and rut formation to traction assistance, via a reduction of ground pressure and slip.

On flat terrain, slip can also strongly contribute to rut formation and soil compaction by shearing off fragments at the wheel–soil interface and by shearing deformation of the soil volume below (Raghavan et al. 1977, Ringdahl et al. 2012), especially in the case of soils with fine texture and high moisture content. High tractive forces of modern powerful machines can not only lead to higher slip at the wheel–soil interface, but inevitably also increase the resulting force of wheel load and tractive force transmitted into the soil (Renius 2020). Thus, the question arises whether traction assistance might also be a feasible means of reducing the disturbance of sensitive soils in flat terrain.

An initial study addressing this question was conducted in 2018 by Schönauer et al. (2020). They observed mean rut depths of only 2.7 cm after six passes of an 8-wheel forwarder with a total mass of 21.5 metric tons on a clay loam soil. No significant difference in rut depth after machine traffic with and without traction assistance was observed, and this was associated with mean wheel slip rates of only 6.2% during unassisted machine travel. A significant influence of external traction assistance on soil compaction was not found either. These observations were attributed to the low average soil moisture content of 27% (volumetric) at the experimental site, resulting from an exceptionally dry summer period prior to the trial in 2018. Therefore, as the conditions did not represent a sensitive soil state, an assessment of the effectiveness of traction assistance on flat terrain was limited. The following research questions were thus addressed in this work:

⇒ To which extent does traction assistance reduce wheel slip of a loaded forwarder on a fine-textured, moist soil in flat terrain?

⇒ To which extent does a reduction of wheel slip also reduce rut formation and soil compaction under such conditions?

2. Materials and Methods

2.1 Study Site

The study was conducted at a forest site located close to the city of Kassel in central Germany (approximate coordinates 9°37'8" E / 51°18'54" N, elevation 350 m a.s.l.), owned by the federal state of Hessen and managed by the state forest service. This site was chosen as it provided a fine-textured soil and a terrain inclination of less than 3.5%. According to the forest inventory and planning documentation, soil type was loamy silt over sandy loam developed from loess sediment, with the fraction of particles larger than 2 mm amounting to only 2% by mass. The forest stand was dominated by oak (*Quercus* spp.) with about 10% beech (*Fagus sylvatica* L.) of an approximate age of 170 years (HessenForst 2018).

2.2 Tested Machines

The forest machine used in this trial was an 8-wheeled forwarder *John Deere 1510G* (Fig. 1a) equipped with tires *Alliance 644 Forestar III* in dimension 710/45-26.5 at an inflation pressure of 3.5 bar (which was the general setting used by the machine operator). For the trial, the forwarder was loaded with softwood logs available on site which resulted in a gross mass of 28.6 t as determined by wheel load measurement using two wheel-load scales *Haenni WL 103*. Measurements were done on the left wheels of the front and rear bogie axle, respectively, and lateral wheel load distribution was assumed to be symmetrical. The basic machine and tire specifications as well as data based on wheel load measurement are provided in Table 1.

During the experiment, the forwarder was driven in all-wheel-drive mode and low gear with all differentials locked; the operator was instructed to drive at a constant speed of 2 km/h (0.56 m/s).

The traction aid winch used was an *Ecoforst T-Winch 10.1* (Fig. 1b), a self-propelled unit on a tracked undercarriage with a diesel engine driving both the winch and the tracks through a hydrostatic transmission. Its basic specifications are given in Table 2. While line speed is automatically synchronized with the travel speed of the tethered machine, tractive force has to be adjusted manually via a potentiometer on a remote-control unit.

In regular operations, winch tractive force is adjusted by the machine operator with an initial setting for a particular work site chosen by experience, with readjustments only being made when slip is perceived during machine travel. For this experiment, wheel slip

Table 1 Basic machine specifications of the forwarder used (John Deere 2019), tire specifications (Yokohama Off-Highway Tires 2021) and data based on wheel load measurement

Basic machine specifications: *John Deere 1510G*	
Maximum engine output, kW	164
Maximum engine torque, Nm	978
Transmission type	Hydrostatic-mechanical, 2-speed gearbox
Tractive force, kN	185
Rated payload, kg	15,000
Minimum operating mass (8-wheeled), kg	18,230
Tire specifications: *Alliance 644 Forestar III*	
Profile type	Traction
Width/diameter (unloaded), cm	71/134
Outer circumference (over lugs), cm	421
Lug height, cm	4.5
Inflation pressure, kPa	350
Measured wheel loads, total mass and nominal ground pressures	
Wheel load, front wheel of front bogie, kg	2800
Wheel load, rear wheel of front bogie, kg	2800
Wheel load, front wheel of rear bogie, kg	4400
Wheel load, rear wheel of rear bogie, kg	4300
Total mass, kg	28,600
*NGP**, front wheels of front bogie, kPa	57.9
NGP, rear wheels of front bogie, kPa	57.9
NGP, front wheels of rear bogie, kPa	90.3
NGP, rear wheels of rear bogie, kPa	88.3

* Nominal ground pressure (Mellgren 1980); calculated as $NGP = G_w / (R \times b)$ where: G_w – wheel load, kg; b – wheel width, cm; R – unloaded wheel radius, cm

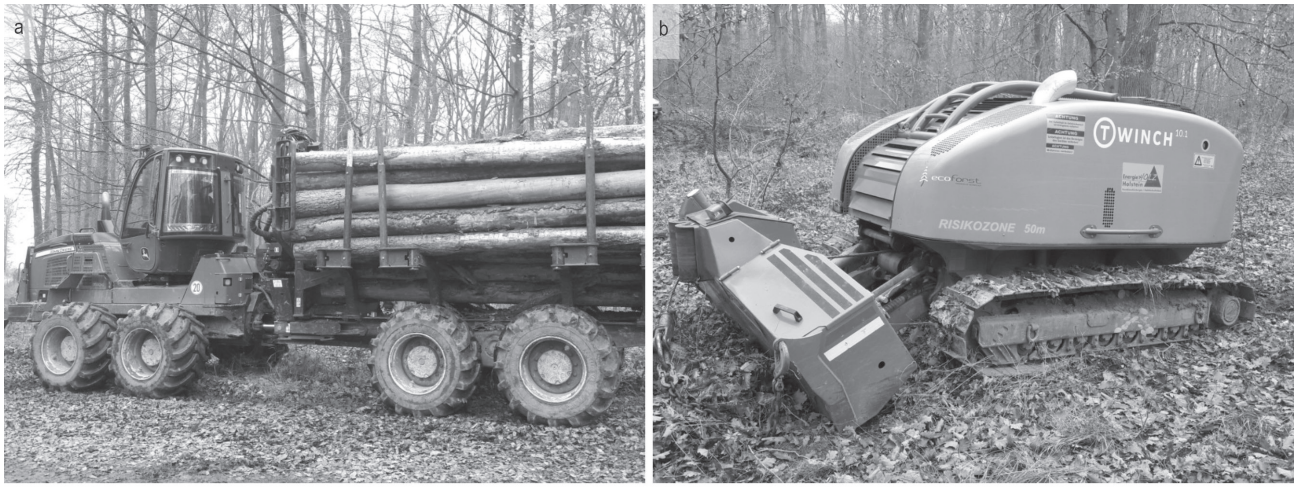

Fig. 1 8-wheel forwarder *John Deere 1510G* (a) and traction aid winch *Ecoforst T-Winch 10.1* (b) used in the trial. The image of the forwarder shows the softwood logs carried during the experiment. The winch is pictured in working position, with the blade lowered against a stump for securing the machine in place during traction assistance

Table 2 Basic specifications of the traction aid winch *Ecoforst T-Winch 10.1* (Ecoforst GmbH 2018)

Basic specifications	
Approximate operating mass, kg	7500
Maximum engine output, kW	107
Maximum tractive force (line pull), kN	80
Maximum line speed, m/s	1.1
Cable length, m / diameter, mm	500 / 18.5

was to be kept as close to zero as possible when driving with traction assistance. Therefore, the winch was not controlled by the machine operator but by a separate person walking along with the slow-moving forwarder, constantly observing the wheel–ground interface and adjusting tractive force to current rut depth and estimated rolling resistance, or occurring wheel slip.

2.3 Experimental Layout

Two experimental plots, one to be crossed by the forwarder without traction assistance (Off-plot) and one to be crossed with traction assistance (On-plot), were established at the study site. These plots were marked out on a relict machine operating trail with a size of approximately 4×30 m each. The machine operating trail was not part of the trail system in use and thus it was assumed that it had not experienced any machine traffic in recent years. The plots were located in sequence, but due to surrounding trees they were not oriented in a straight line. Sufficient distance was kept between them so that the forwarder could be aligned before entering the second plot, thus avoiding steering movements while travelling along this plot. The plots were cleared of debris, and the organic layer above the mineral soil was removed since the loose and rough surface and the potentially elastic behaviour of this layer would have interfered with the rut depth measurements.

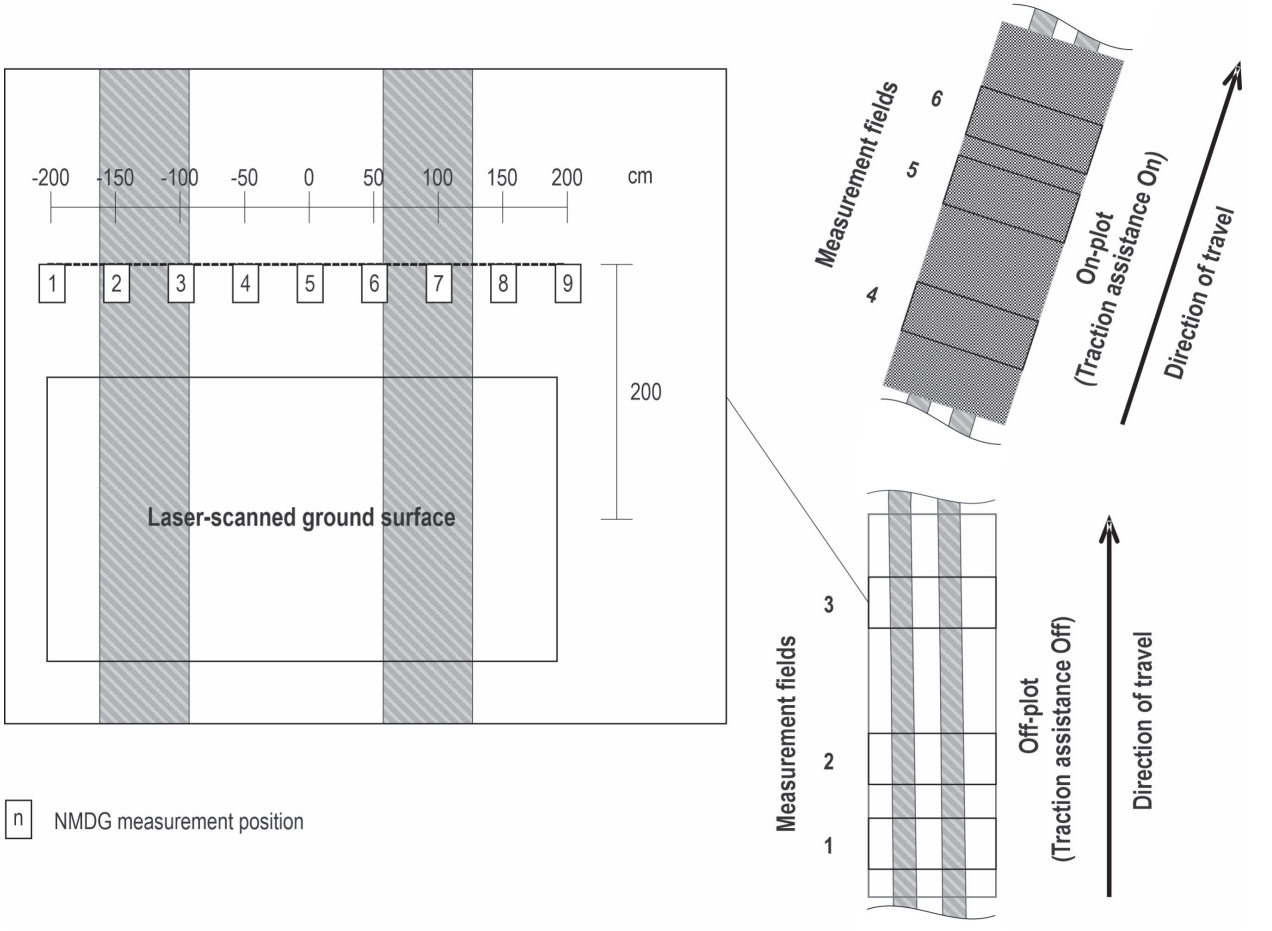

Fig. 2 Spatial layout of the experiment. Each set of nuclear moisture and density gauge (NMDG) measurement transect and laser-scanned ground surface is denoted as a measurement field. Each of the two test plots included three of these measurement fields. The relative location of the wheel tracks generated during the experiment is indicated by the grey striped lines

For each of the two plots, three locations for the measurement of soil physical properties and for laser scans of the ground surface, subsequently referred to as measurement fields, were selected and marked out. The measurement fields were not equidistantly placed within each plot, but their positions had to be chosen so that there was sufficient clearance to surrounding trees. Fig. 2 presents a schematic view of the spatial layout.

2.4 Preparation of Plots

The experiment was conducted during four days in late November 2020. Due to the precipitation deficit of the preceding three years, soil moisture content was low, implying an unusually low susceptibility of the soil to plastic deformation despite its fine texture. Thus, watering of the plots was deemed necessary to obtain adequate soil conditions for the experiment, and this was carried out during two days preceding the experiment. On each of these two days, approximately 10 m^3 of water were spread on each of both plots via sprinklers and perforated hoses. Thus, each experimental plot with an area of roughly 120 m^2 received approximately 20 m^3 of water, corresponding to 167 mm of precipitation. Soil moisture readings on the second day of the experiment using a soil moisture sensor Delta-T Devices ML3 ThetaProbe showed mean volumetric soil moisture contents of 40.3% in the Off-plot (standard deviation 3.7%, range 34.2–46.9%) and 42.8% in the On-plot (standard deviation 7.8%, range 28.8–55.2%).

2.5 Measurements

2.5.1 Soil Texture Analysis and Standard Proctor Tests

For analysis of soil texture (particle size distribution) and standard Proctor tests, two disturbed soil samples were taken from the study site, one within each of the plots. Analysis of particle size distribution was done following the requirements of DIN EN ISO 17892-4:2016 (DIN 2017), applying the improved integral suspension pressure method (Durner and Iden 2021) by using a PARIO soil particle analyzer (METER Group AG 2021) and wet sieving. Standard Proctor tests to estimate maximum dry density as a reference for the compaction state of the soil pre- and post-impact were carried out according to DIN 18127:2012-09 (DIN 2012).

2.5.2 Soil Density and Gravimetric Moisture Content

Repeated measurement of soil wet density, gravimetric moisture content and dry density (bulk density) was performed with a Troxler 3440 nuclear moisture and density gauge (NMDG). Wet density and gravimetric moisture content (absolute, i.e. in g/cm^3) are directly measured by a NMDG via the attenuation of gamma radiation and the moderation (thermalization) of neutron radiation, respectively, and dry density is then automatically calculated as the difference of these measurements (Labelle and Jaeger 2021). As indicated in Fig. 2, NMDG measurements were done on one transect in each measurement field. On each transect, nine fixed measurement positions with a spacing of 50 cm were established by pre-boring vertical holes for insertion of the probe of the NMDG down to its maximum measurement depth of 30 cm. Measurements were done at 10, 20 and 30 cm depth. The first measurement time was pre-impact, one day before the first machine pass, and subsequent measurement time points were after 3, 7 and 15 machine passes, respectively, implying one-day intervals between measurements. Plastic tubes with the same diameter as the probe of the NMDG were inserted in the holes between the measurements to prevent backfilling due to machine traffic.

2.5.3 Rut Depth

Laser scanning of sections of the ground surface in both plots was done to monitor rut formation due to machine travel. A downward-facing fan-beam laser scanner Triple-IN PS100-90 travelling along an aluminum beam supported by two tripods on fixed positions was used (see Fig. 3a). As illustrated in Fig. 2, ground-surface scans were performed in each of the three measurement fields in each plot, and after the initial scans pre-impact they were repeated after every machine pass for the first seven passes and then again after the 10^{th} and 15^{th} pass. Resulting from the angle of aperture of the laser scanner of 90° and its height above ground, the length of the scanned segments, i.e. their extent along the main axis of the plots (direction of machine travel) was approximately 3 m. Their width corresponded to the distance travelled along the beam, and, with fixed start and end points, it was approximately 4 m for each scan. The position and height of each set of two tripods (one set in each measurement field, six sets in total) defined the reference plane for the ground-surface scans and was thus kept constant throughout the experiment.

Raw data obtained from the ground-surface scans were point clouds representing vertical distance of each point from the reference plane, i.e. depth maps. These depth maps were processed with a proprietary software that allowed visualization such as greyscale images and manual segmentation (see Fig. 3b). In order to extract a mean depth for each rut at each measurement time point, segments centered within the left

and right wheel tracks and with sufficient clearance to the edges of the ruts to avoid interference from lose soil or debris were defined as indicated in Fig. 3b. The mean depth within each of those two segments was determined for each scan, and the differences between these mean depths at a certain measurement time point and the mean depths from pre-impact measurement (the reference), were taken as rut depths at this measurement time point. As the difference in rut depth between the left and right wheel tracks was not within the scope of this study, the mean of these rut depths was used in further analysis as the rut depth for each measurement field after each traffic increment.

2.5.4 Wheel Slip

Wheel speed and travel speed (true speed over ground) of the forwarder were simultaneously measured using two rotary encoders Kübler Sendix 5000 in assemblies mounted on the forwarder (cf. Schönauer et al. 2020). The rotary encoder used for wheel speed measurement was attached to the rear wheel on the right side of the front bogie axle. Wheel (tangential) speed was calculated from the recorded wheel rotational speed and the measured circumference of the wheel. The second rotary encoder was coupled to a capstan-type reel with a thread fastened to a fixed point, in this case, a tree. Due to unwinding of the thread when the forwarder was moving, rotation of the reel was captured by the rotary encoder, and travel speed was calculated from rotational speed and reel circumference. Both travel speed and wheel speed were simultaneously recorded by a data logger HBM Quantum MX840 at intervals of approximately 65 milliseconds. The travel speed signal showed considerable noise, i.e. high-frequency fluctuations with an amplitude of almost the same magnitude as the average travel speed of approximately 0.6 m/s due to oscillation of the thread, and therefore it was necessary to smooth the speed signals. A moving average filter corresponding to a time interval of approximately 1 s (spanning 16 single readings) was applied to both travel and wheel speed signals. For the calculation of wheel slip, only the readings between the time stamp when a travel speed of 0.5 m/s was first attained and the time stamp when travel speed ultimately dropped below 0.5 m/s were taken from the smoothed speed signals to exclude the acceleration and decceleration phases, which resulted in measurement periods of slightly varying durations. Wheel slip at each time stamp was calculated according to

$$WS = \left(1 - \frac{v_t}{v_w}\right) \cdot 100 \quad (1)$$

Where:

WS wheel slip, %

v_t travel speed, m/s

v_w wheel speed, m/s.

2.5.5 Winch Tractive Force

Winch tractive force was measured using a load cell HBM U2B with a measurement range of 0–200 kN, mounted between the cable of the traction aid winch

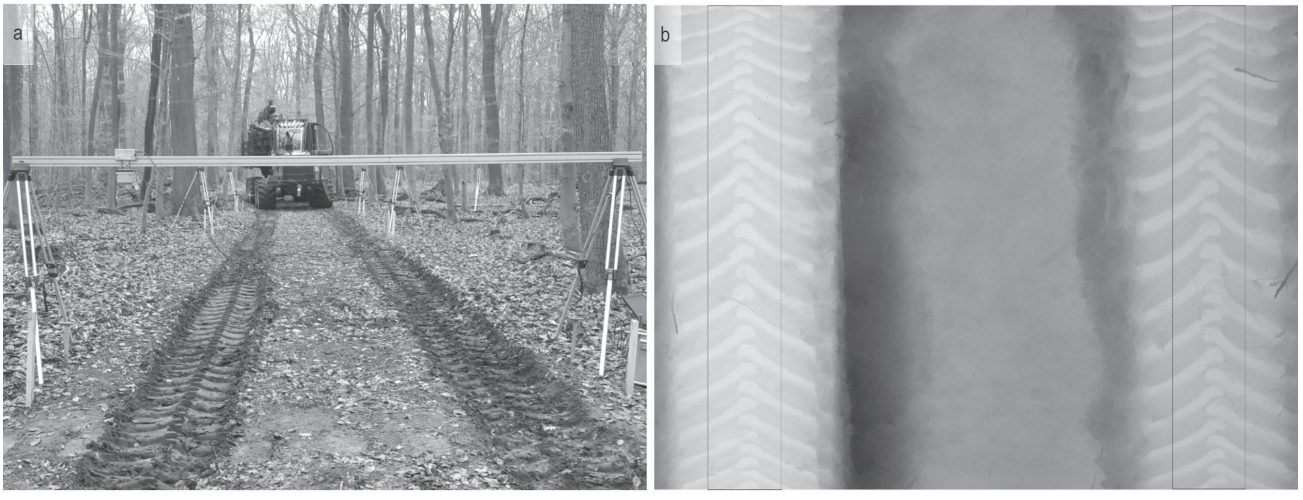

Fig. 3 Set-up of the fan-beam laser scanner used for rut-depth measurement (a) and depth map obtained from scanning in measurement field 3 after 15 machine passes (b). Pixel intensity corresponds to the depth of the point (distance from the reference plane) with higher intensity indicating greater depth. The thin rectangles in the centre of the wheel tracks define the segments used for determination of mean rut depth

and the front towing eye of the forwarder. Recording of winch tractive force was synchronized with recording of travel speed and wheel speed when driving over the On-plot, i.e. tractive force readings were captured with the same frequency and at the same time stamps as the speed signals. The same moving average filter spanning 16 single readings (1 s) as for the speed signals was applied to the tractive force signals.

2.6 Data Analysis

Data processing and analysis was performed using Microsoft Excel and the R language and environment (R Core Team 2021) combined with RStudio (RStudio Team 2021). The lme4 (Bates et al. 2015) and lmerTest (Kuznetsova et al. 2017) packages were used when applying mixed-effects models on the data, and diagrams were prepared using the ggplot2 package (Wickham 2016).

3. Results

3.1 Soil Properties

3.1.1 Soil Texture and Maximum Dry Density

Soil textural class according to DIN 4220:2020-11 (DIN 2020) was silt with medium clay content in both plots, with the percentages of sand, silt and clay varying only slightly between the plots. Sand, silt and clay fractions accounted for 13%, 72% and 15% of particle mass in the Off-plot, while in the On-plot percentages of the fractions were 18%, 66% and 16%, respectively. A soil texture with high susceptibility to deformation was thus confirmed for the plots.

Similar to soil texture, maximum dry density and corresponding optimum moisture content according to standard Proctor tests showed little variation between plots. For the Off-plot, a maximum dry density of 1.66 g/cm^3 at an optimum moisture content (OMC) of 17% was estimated, while for the On-plot, a maximum dry density of 1.66 g/cm^3 at 15% moisture was estimated.

3.1.2 Pre-impact Soil Density and Gravimetric Moisture Content

The NMDG measurements carried out pre-impact indicated that initial soil density and gravimetric moisture content differed between the measurement fields in the Off-plot and those in the On-plot. Descriptive statistics of wet density, absolute and relative gravimetric moisture content and dry density for both plots are given in Table 3. As can be seen, dry density was higher and relative moisture content was lower for the measurement fields in the Off-plot. Regarding the measurements from all nine positions on each transect, these differences were highly significant according to Welch two-sample *t*-tests. Considering only the positions on the transects, which were located directly within the wheel tracks – these being positions 2 and 3 in the left track and position 7 in the right track, consistent for all six transects – the difference in dry density between the transects in the On-plot and those in the

Table 3 Descriptive statistics of pre-impact NMDG measurement of soil density and gravimetric moisture content (MC)

		All transect positions (positions 1–9)		Positions in tracks (positions 2, 3 and 7)	
		Off-plot	On-plot	Off-plot	On-plot
Wet density, g/cm^3	Mean, SD	1.66 (0.15)	1.57 (0.19)	1.61 (0.13)	1.59 (0.15)
	Range	1.32–1.94	1.06–1.89	1.34–1.89	1.28–1.80
MC, g/cm^3	Mean, SD	0.40 (0.06)	0.42 (0.07)	0.40 (0.06)	0.45 (0.04)
	Range	0.32–0.54	0.25–0.53	0.32–0.50	0.38–0.53
MC, %	Mean, SD	32.5 (5.9)	37.1 (8.3) ***	32.8 (5.3)	40.7 (8.1) ***
	Range	24.0–52.1	17.6–63.4	24.0–44.3	29.6–63.4
Dry density, g/cm^3	Mean, SD	1.25 (0.14)	1.16 (0.17) ***	1.21 (0.11)	1.14 (0.16) ·
	Range	0.94–1.55	0.72–1.49	0.96–1.41	0.79–1.34
Relative dry density, %	Mean, SD	75 (8)	70 (10)	73 (7)	69 (10)
	Range	57–93	43–90	58–85	48–81
	N	81	81	27	27

Symbols indicating the significance of differences between Off- and On-plots are coded according to *P*-values of Welch two-sample *t*-tests as follows:
*** <0.001, ** <0.01, * <0.05, · <0.1

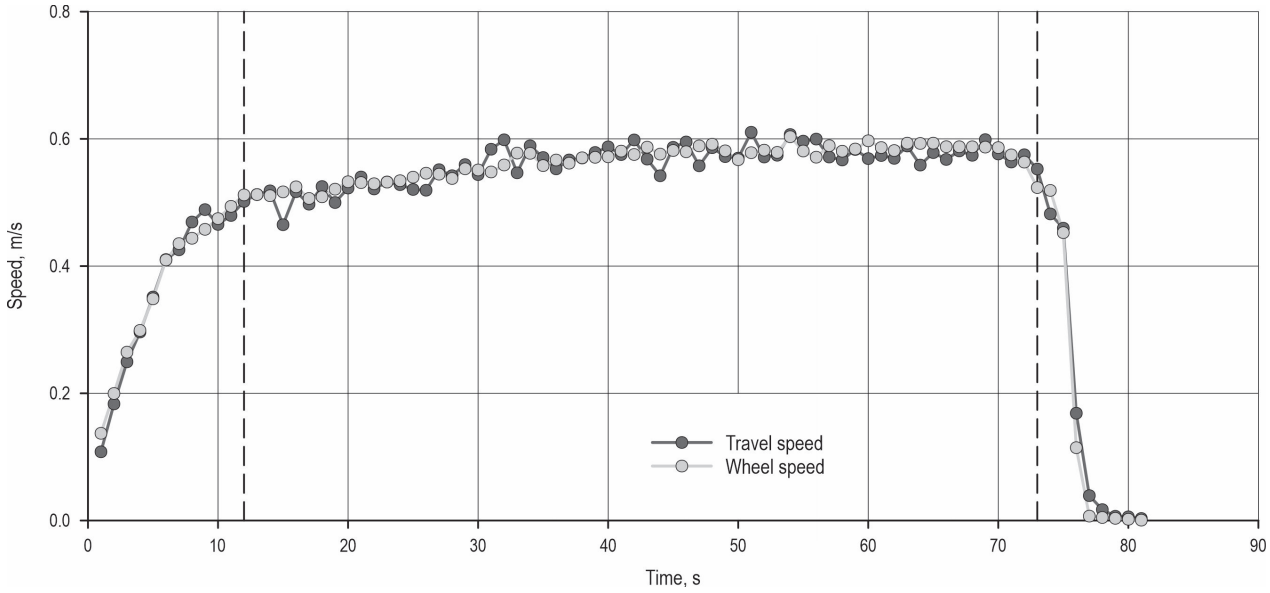

Fig. 4 Smoothed time curves of travel speed and wheel speed (one-second mean values) for the 5th machine pass with traction assistance. Vertical lines delineate the part of the curves used for calculation of mean wheel slip

Off-plot was only marginally significant (*P*-value <0.1 but >0.05), while the corresponding difference in relative moisture content remained highly significant.

The relative dry densities (also referred to as relative bulk densities) indicated in Table 3, i.e. the measured dry densities expressed as percentages of the estimated maximum dry density, suggest a moderately high degree of soil compaction on the plots in the context of root–soil interaction and related plant growth. Relative dry densities beyond approximately 80% were found to reduce growth both in agricultural crops and coniferous trees (Carter 1990, Zhao et al. 2010).

3.2 Wheel Slip and Winch Tractive Force

Time curves of travel speed and wheel speed are exemplarily shown for the 5th machine pass with traction assistance in Fig. 4. As can be seen, wheel speed was slightly higher than travel speed during a large part of the monitored time, equaling positive slip, but short sequences of the opposite case, i.e. negative slip, were also present. Such momentary alternation between positive and negative slip was distinctive for the machine passes with traction assistance. In contrast, during machine passes without traction assistance, wheel speed was typically higher than travel speed for extended periods and negative slip only occurred for isolated one-second mean values. Here, it has to be noted that some noise in the travel speed signal may have persisted even after filtering, leading to a slight overestimation of travel speed. While the actual slip may thus have been underestimated, such bias would be systematic and would therefore not affect the comparison between unassisted and assisted travel.

As stated in the description of the tested machines, winch tractive force was manually adjusted during each machine pass with traction assistance, attempting to obtain practically zero slip. Exemplifying the interaction of tractive force and wheel slip that resulted from this approach, time curves of both variables during the 15th machine pass with traction assistance are shown in Fig. 5. It can be seen that gradually increasing winch tractive force from approximately 44 kN to more than 60 kN during the forwarder travel at speeds greater than 0.5 m/s coincided with measured wheel slip shifting from mostly positive to mostly negative values. Even in the case of slightly biased slip values, periods of minimal negative slip (skid) may have actually occurred, as was visually observed and perceived by the machine operator. In any case, a reduction of slip through the winch tractive force is recognizable.

Analysis of all 15 machine passes with and without traction assistance showed that mean wheel slip almost steadily increased with each pass when driving unassisted, rising from 1.9% for the first pass to 8.0% for the 15th pass, as can be seen in Fig. 6.

When traction assistance was provided during travel over the On-plot, on the other hand, mean wheel slip did not exceed 1.0% for any of the 15 passes. Slightly negative mean wheel slip occurred in two more cases in addition to the 15th pass. As the exemplary time curves of speeds and wheel slip suggested, momentary variation of slip was very pronounced.

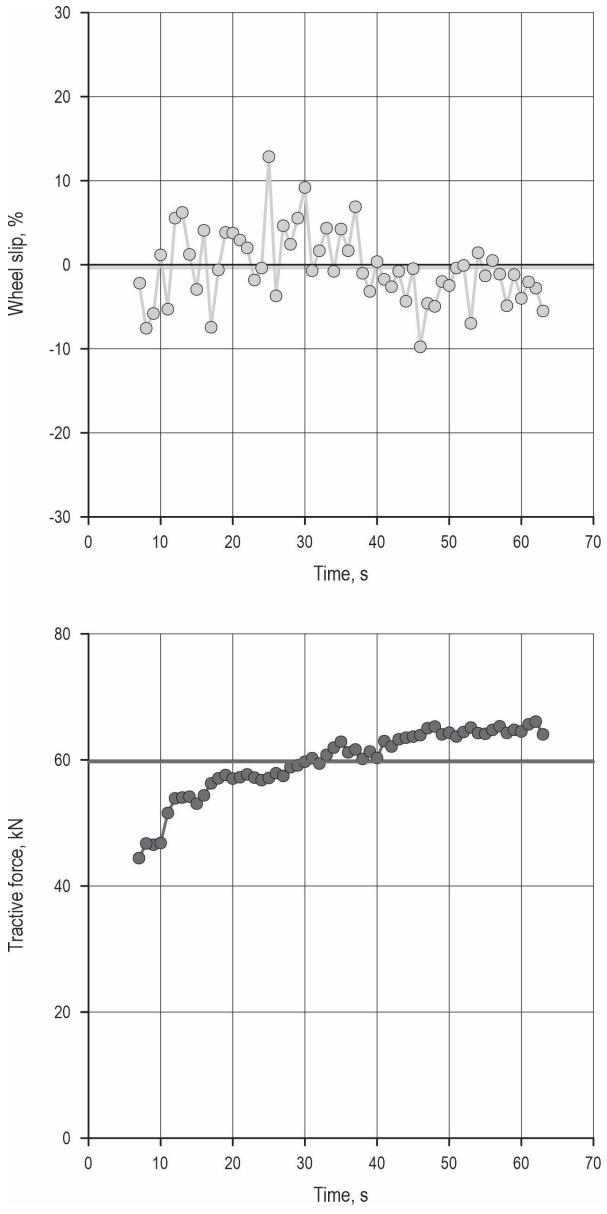

Fig. 5 Time curves of wheel slip and winch tractive force during the 15th machine pass with traction assistance. Bold horizontal lines in both panels indicate the mean of all one-second mean values

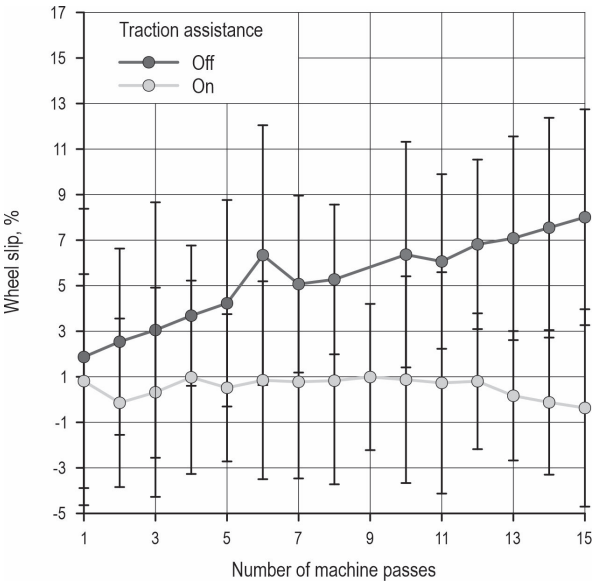

Fig. 6 Wheel slip during travel with and without traction assistance (i.e. over the Off- and On-plots) plotted against the number of machine passes. The points and whiskers represent mean and standard deviation of one-second mean values of wheel slip for each machine pass. Missing values for the 9th pass over the Off-plot are due to incomplete recording

This is reflected in the large standard deviations indicated in Fig. 6.

In a linear model of the form:

$$WS = \beta_0 + \beta_1 \cdot NP + \beta_2 \cdot TA + \beta_3 \cdot NP \cdot TA + \varepsilon \quad (2)$$

Where:

WS wheel slip as one-second mean values, %
NP number of machine passes (covariate)
TA traction assistance (factor with two levels, Off and On)
$\beta_{0–3}$ intercept and coefficients
ε residual variance.

All parameters were highly significant (Table 4). This indicates that, despite the large variation of wheel

Table 4 Summary of the specified linear model of wheel slip

Variable	Coefficient estimate	Standard error	*t*-value	Probability (*P*-value)	Significance
(Intercept)	2.116	0.303	6.989	$3.87 \cdot 10^{-12}$	***
NP	0.399	0.033	12.061	$<2\ 10^{-16}$	***
TA: On	–1.399	0.416	–3.367	$7.76 \cdot 10^{-4}$	***
NP *TA*: On	–0.422	0.046	–9.190	$<2 \cdot 10^{-16}$	***

R^2: 0.280; R^2 (adjusted): 0.278
F-statistic: 237 (degrees of freedom: 3 and 1832); *P*-value: $<2.2 \cdot 10^{-16}$
Symbols indicating the significance of coefficient estimates are coded according to *P*-values as follows: *** <0.001, ** <0.01, * <0.05, . <0.1

slip during machine passes, wheel slip can generally be expected to be higher and to increase with every machine pass over the same track when driving without traction assistance under soil conditions similar to this trial.

Fig. 7 shows the interaction between mean wheel slip and mean winch tractive force for each of the machine passes with traction assistance. It can be noted that mean winch tractive force was raised by more than 500% during the experiment, from an initial 9.4 kN to 59.7 kN for the 15th machine pass. At the same time, mean wheel slip showed little variation, remaining between 0.5% and 1.0% when mean winch tractive force increased from 23.1 kN to 39.6 kN during passes 4–12 and attaining only minimally negative values for the last two passes with high winch tractive forces. An apparent increase of traction assistance required for virtually no slip with repeated traffic over the same track, as indicated by this observation, can be seen in relation to the increasing slip observed with the increasing number of machine passes without traction assistance. Both might be explained by the increasing loss of soil strength and increasing rolling resistance with increasing rut depth.

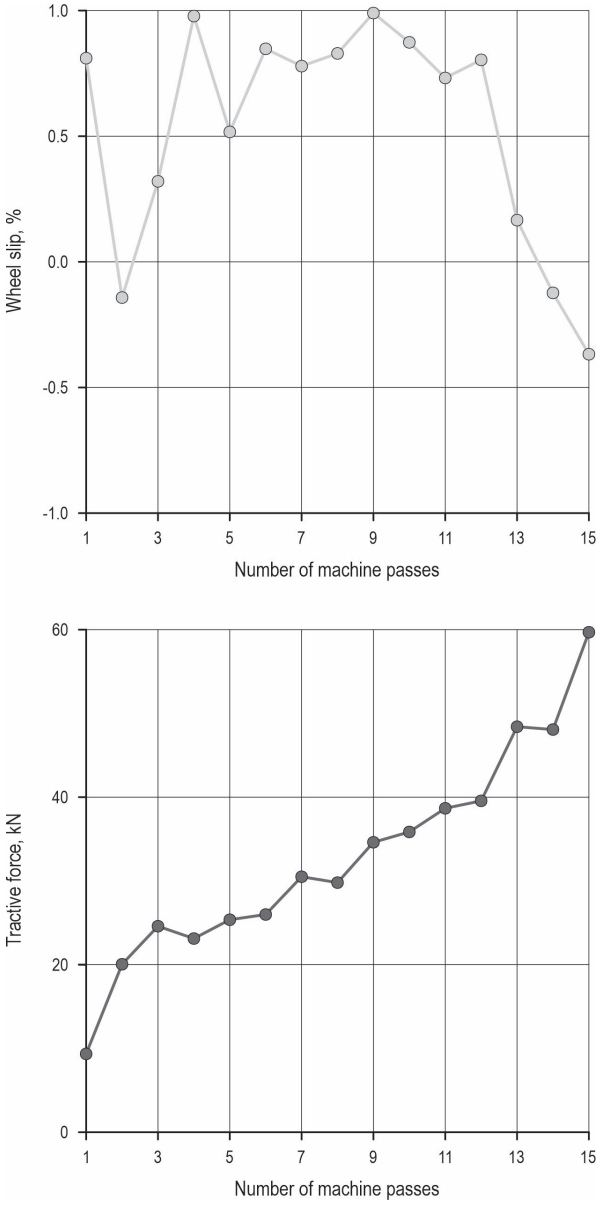

Fig. 7 Mean wheel slip and mean tractive force during travel with traction assistance (i.e. over the On-plot) plotted against the number of machine passes

3.3 Rut Depth

Mean and standard deviation of rut depth in the Off- and On-plots at each time of measurement are indicated in Table 5. With mean rut depths after 15 machine passes of 12.3 cm for the Off-plot and 8.6 cm for the On-plot, mean rut depth increments per machine pass were 0.82 cm and 0.57 cm, respectively.

However, the development of rut depth in the individual measurement fields within the plots differed considerably as shown in Fig. 8, with the discrepancy between measurement fields 1 and 3 in the Off-plot being most pronounced. Remarkable with this dissimilar development of rut depth was that neither initial soil dry density nor initial moisture content in the wheel tracks exhibited any marked difference between the two measurement fields, these being 1.20 g/cm^3 for measurement field 1 versus 1.21 g/cm^3 for measurement field 3 and 34.1% versus 35.6%, respectively. In the case of the On-plot, differences between the measurement fields were less distinct.

Table 5 Mean and standard deviation of rut depths in the Off- and On-plots at each time of measurement

Number of machine passes	Rut depth, cm	
	Off-plot	On-plot
1	2.4 (0.6)	1.7 (0.0)
2	3.3 (1.0)	2.7 (0.0)
3	4.2 (1.2)	3.4 (0.1)
4	4.9 (1.4)	4.0 (0.3)
5	5.8 (1.5)	4.5 (0.4)
6	6.5 (1.9)	5.1 (0.5)
7	7.3 (2.1)	5.6 (0.5)
10	9.3 (2.5)	7.1 (0.8)
15	12.3 (2.7)	8.6 (1.2)

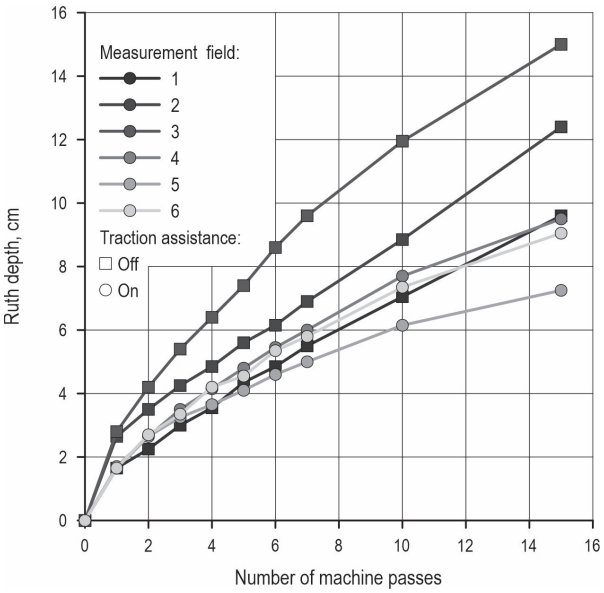

Fig. 8 Development of rut depth in measurement fields in both plots

Mixed-effects models were specified to assess whether the observed difference in rut formation between the Off- and On-plots was significant, i.e. whether traction assistance can be expected to reduce rut formation in general under conditions comparable to those on the test plots. Considering both the large differences in rut formation observed among the measurement fields and the situation that the measurement fields for each of the treatments were spatially nested within the plots, random effects with the measurement field number as grouping variable were included in the models. Both linear mixed-effects models (LMM), i.e. models fitted to Gaussian distributions, and generalized linear mixed-effects models (GLMM) were tested. In the latter case, the models were fitted to gamma distributions since only positive rut depth values are expected with the measurement method applied in this study and since the ratio of mean and standard deviation remained almost constant for rut depth with increasing number of machine passes (cf. Salmivaara et al. 2020). The best fit (maximum likelihood) among the tested models meeting the assumption of normally distributed and homoscedastic residuals was observed with a second-order polynomial GLMM with identity link and the following specification:

$$RD = (\beta_0 + u_{0,i}) + (\beta_1 + u_{1,i}) \cdot NP + \beta_2 \cdot NP^2 + \beta_3 \cdot TA + \varepsilon \quad (3)$$

Where:

RD rut depth, cm
NP number of machine passes (covariate)
TA traction assistance (factor with two levels, Off and On)
$\beta_{0–3}$ fixed-effect intercept and coefficients
$u_{0–1,I}$ random-effect intercept and coefficients for measurement field i
ε residual variance.

Table 6 presents a summary of this model. As can be seen, the effect of traction assistance was not significant.

Apparently, in contrast to the number of machine passes, the use of traction assistance under the given conditions does not inherently influence rut depth.

Table 6 Summary of specified GLMM of rut depth

Fixed effects (predictors)	Coefficient estimate	Standard error	*t*-value	Probability (*P*-value)	Significance
Intercept	1.421	0.256	5.557	$2.74 \cdot 10^{-8}$	***
NP	0.956	0.105	9.069	$<2 \cdot 10^{-16}$	***
NP^2	–0.018	0.002	–11.295	$<2 \cdot 10^{-16}$	***
TA: On	–0.219	0.393	–0.557	0.578	–
Random effects	Variance	–	–	–	–
Intercept	0.054	–	–	–	–
NP	0.008	–	–	–	–
Residual	0.004	–	–	–	–
Fit		–	–	–	–
Log-likelihood	–2.7	–	–	–	–
AIC	21.4	–	–	–	–
BIC	37.4	–	–	–	–

Symbols indicating the significance of coefficient estimates are coded according to *P*-value as follows: *** <0.001, ** <0.01, * <0.05

Variation in soil conditions between the six measurement fields and also between the two plots presumably had a strong influence on rut formation at individual locations.

3.4 Soil Compaction

For assessing the effect of machine traffic with and without traction assistance on soil density, only the measurement positions in the tracks (positions 2, 3 and 7 on each of the transects) were regarded since these positions were within the contact area of the tires and, as such, directly affected by the wheel loads. Fig. 9 shows wet density, moisture content and dry density plotted against the number of machine passes, with mean values indicated for each of the six transects.

It can be noted that a marked increase in wet or dry density only occurred during the first three machine passes. Mean dry density in the Off-plot increased from an initial 1.21 g/cm^3 to 1.44 g/cm^3, while in the On-plot an increase in mean dry density from 1.14 g/cm^3 to 1.28 g/cm^3 was observed. This corresponds to increases in relative bulk density from 73% to 87% and from 69% to 77%, respectively. The values measured after the 7th and 15th machine pass appear anomalous. The measurement after the 7th pass showed virtually no further increase in wet density combined with a rise in moisture content. Thus, decreasing dry densities resulted for this measurement time. This did not seem plausible, particularly, as the individual readings from 30 cm depth exhibited the same behavior (data not shown). A potential loosening effect of the moving wheels on the top soil was not assumed to extend to greater depths in the soil. If an actual increase in moisture content had occurred, an increase should have been observed in the wet density measurements as well. Considering the known sensitivity of the NMDG to the presence of organic matter in the shallow area of influence for moisture content measurement (cf. Labelle and Jaeger 2021), one explanation for the observed fluctuation of moisture content could be the displacement of organic material such as fine roots within this area of influence. As a consequence, only the measurements recorded pre-impact and after the 3rd machine pass were considered for further analysis.

In Fig. 10 absolute change in dry density after the 3rd machine pass is plotted against pre-impact dry density for each individual measurement (position and depth).

Apparently, density increases were higher in the Off-plot. Mean density increase for all depths combined was 0.23 g/cm^3 for the Off-plot and 0.14 g/cm^3 for the On-plot. The difference was significant according to a Welch two-sample *t*-test (P<0.001). When

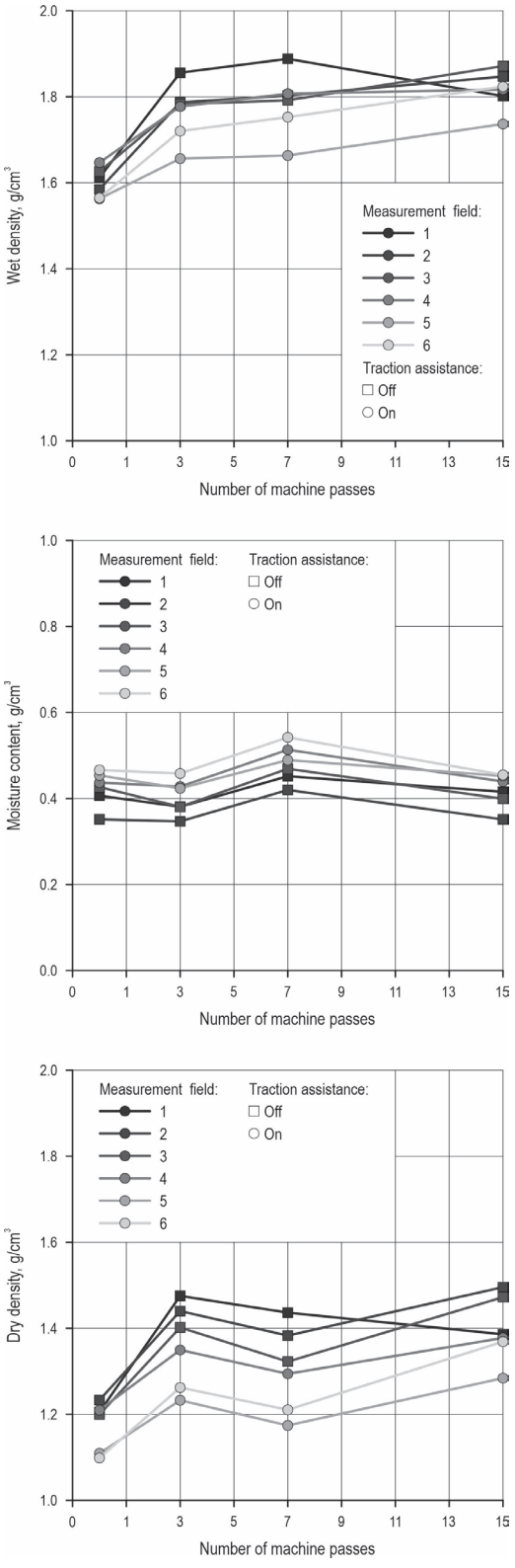

Fig. 9 Mean soil wet density, gravimetric moisture content and dry density for transects in both plots at each NMDG measurement time. Mean values from measurement positions under wheel tracks are indicated for each transect

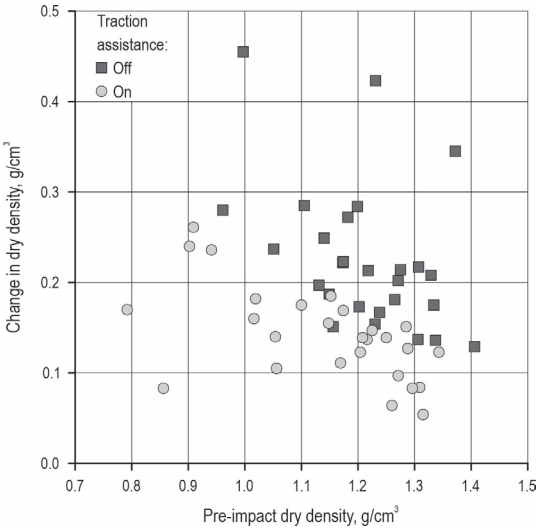

Fig. 10 Change in dry density after the 3rd machine pass plotted against pre-impact dry density for individual measurements (positions and depths) under wheel tracks in both plots

regarding the measurement depths separately, differences in density increases were significant for the depths of 20 cm and 30 cm (P=0.011 and P=0.002), but not for the depth of 10 cm (P=0.130). In this context, it has to be noted that the observed density increases might have been influenced to some extent by an increase in actual measurement depth. Due to the NMDG measurement positions being located in the ruts, any target measurement depth was increased by rut depth in relation to the initial reference level. As a reference, the mean increase in pre-impact dry density from 10 to 20 cm depth was 0.16 g/cm^3, while it was 0.08 g/cm^3 from 20 to 30 cm depth. However, as plot-wise mean values of rut depth after the 3rd machine pass did not differ markedly between the Off- and On-plot (4.2 versus 3.4 cm), the potential influence of increased measurement depth was presumably not different between the plots.

4. Discussion

Mean wheel slip during unassisted travel was remarkably low even during the final machine pass. As mentioned before, this may partly be attributed to a slight underestimation of slip as a consequence of the noisy travel speed signal. As an orientation, Ringdahl et al. (2012) observed 10–15% wheel slip for a forwarder on forest terrain (albeit with snow cover and with bogie tracks on both axles) and assumed this to be a common magnitude. In the context of agricultural machines, wheel slip in the range of 20% is still accepted as »usual« (Raghavan et al. 1977) since the highest tractive effort is assumed to be produced in this slip range on dry, paved surfaces, with ultimate tractive effort on soils occurring only at slip values of 50% and beyond (Renius 2020). Interesting and somewhat contradictory to the low slip rates during unassisted travel was the observation that a rather strong increase of winch tractive effort was apparently required with the increasing number of machine passes to keep slip virtually at zero. Probably slip rates could have been kept within a range still regarded as negligible from a practical perspective with considerably less tractive force, but it is still noticeable that a tractive force of more than 40 kN, i.e. more than 50% of the capacity of the winch, was required for virtual no-slip conditions during the last three machine passes. As a reference, Holzfeind et al. (2019) observed mean cable tensile forces in the range of 27 to 56.8 kN for a John Deere 1210E forwarder with a total mass of 31.4 t at nominal payload working on a slope where mean inclination of the machine varied between 22% and 52%. This indicates for the original application of traction aid winches, i.e. operations in steep terrain, that a further reduction of soil disturbance by providing greater traction assistance than commonly applied in practice might be possible. In this context, upgrading traction aid winches with systems for slip detection and automatic adjustment of tractive effort instead of operating them with manually preset tractive effort might be an interesting concept, albeit with accurate real-time slip measurement presumably still posing a challenge (Ringdahl et al 2012).

Considering the high number of machine passes and the deformable state of the soil indicated by mean soil moisture contents above the estimated OMC of 15–17%, final rut depth on both plots was unexpectedly low. Compaction from historic machine traffic, as suggested by pre-impact relative bulk densities of approximately 70% (of the estimated maximum dry density) on average, may have contributed to this observation. A lower mean soil moisture content throughout the Off-plot might have lessened the effect of traction assistance. Two of the measurement fields in the Off-plot still showed considerably greater rut depth after any traffic increment than the measurement fields in the On-plot. However, in one measurement field in the Off-plot, rut depth was well within the range of those in the On-plot, and as a result the effect of traction assistance on rut formation was not found significant. As an explanation for the dissimilar behavior of the measurement fields in the Off-plot, inhomogeneity within the soil can be assumed, possibly local variation of soil reinforcement through the root network

(Wästerlund 1989) and varying soil depth atop the bedrock. During and after the trial, it was visually observed that no soil material was entirely sheared off at the surface and moved to the sides of the tracks by the tire lugs. Rather, the formation of lateral bulges seemed to conform to the soil failure mechanism described initially by Prandtl's theory, and soil displacement thus occurred as a process of interacting compaction and shear displacement (Bachmann et al. 2014, Wiberg et al. 2021).

So far, the inconclusive results of the study do not allow for a recommendation to use traction assistance on sensitive soils in flat terrain. In this context, the effort made to keep wheel slip close to zero by manually adjusting traction assistance according to visually observed and previously measured slip has to be noted. Such an approach is not feasible in practical operations, and thus the effectiveness of traction assistance would likely be lesser in practice with current equipment.

Increased soil compaction observed with unassisted travel as compared to the situation with traction assistance might be explained by higher shear stress in the soil due to a higher resultant force, i.e. higher peak contact pressure. When travelling unassisted (with the same wheel loads) a higher tractive force has to be generated at the wheel–soil interface to maintain vehicle speed (Renius 2020). This assumption is consistent with the observation of higher slip values for unassisted travel, as increased soil compaction can be expected with higher slip up to a certain point according to literature. Raghavan et al. (1977) reported that soil compaction due to vehicle traffic was highest at slip rates between 15 and 25% in field tests, apparently at the point of maximum shear stress that the tested soils could withstand. Beyond this slip range, the authors observed the soils to be sheared off.

The observation that the strongest increase in soil dry density occurred during the first three machine passes, while there was only minimal change in dry density from the 3rd to the 15th machine pass despite the much higher additional cumulated load, might indicate that soil deformation shifted from compaction to prevailing shearing displacement early in the course of repeated traffic. Considering that soil moisture contents were above OMC, such a behavior of the soil seems plausible, and it is also consistent with observations in previous studies, e.g. those by Froehlich (1978), McNabb et al. (2001) or Ampoorter et al. (2007). An interesting side note is the fact that already in the work by Foehlich (1978), where a NMDG was also used for repeated soil density measurements, decreasing densities with additional machine passes after initial compaction were noticed and this behavior was attributed to the measurement method.

Concerning the accuracy of the measurements, potential for improvement was identified with two of the methods employed. Due to the possible overestimation of soil moisture content with NMDG measurement, it should be complemented with a limited number of soil cores samples. Furthermore, for repeated measurement in wheel ruts with progressive depth, attempting to maintain a constant measurement depth in relation to the initial ground surface might be advisable, i.e. starting at a rather great measurement depth and incrementally reducing probe insertion depth to compensate for the increasing rut depth. Regarding wheel slip measurement, negative momentary slip values still persisting in the measurement data of unassisted travel after smoothing can be seen as implausible. Even if their occurrence was infrequent and thus not deemed to have substantially biased the results, an alternative method of travel speed measurement excluding the mentioned problem with an oscillating thread would be desirable.

5. Conclusions

Under the conditions of this trial, only moderate wheel slip was observed with unassisted travel, even after a high number of repeated passes in the same track with a heavy forwarder. Thus, no excessive soil deformation occurred due to soil shear-off at the surface with rapid deepening of the wheel ruts. With traction assistance, wheel slip could be kept below 1%, and the tractive force applied to maintain this condition showed a strong increase with the increasing number of machine passes. Both reduced rut depth and reduced soil compaction were observed with traction assistance, but only the latter was found significant. The observed relationships between slip, rut formation due to shear displacement and soil compaction are consistent with soil mechanics theory. To assess whether the non-significant difference in rut formation was due to inhomogeneity of the forest soil and thus whether a reduction of soil displacement can be effectively achieved with traction assistance, repeating the experiment under more homogenous soil conditions without a dense network of tree roots, e.g. on an agricultural field or a pasture, should be considered. Ideally, this would be complemented with further tests under varying soil conditions including higher moisture contents and different textural classes. A clear understanding of the effectiveness of traction assistance in flat terrain would then allow for judging this technique in relation to other means of soil disturbance mitigation.

Acknowledgements

This research received funding through the Bio-Based Industries Joint Undertaking under the European Union's Horizon 2020 TECH4EFFECT project (grant agreement 720757) and from the Eva Mayr-Stihl Stiftung. The authors want to express their gratitude to HessenForst for providing the test site and for financially supporting the field experiment. The authors also thank Mr. Markus Müller for general support and for aid in finding a test site, Mr. Frank Holstein for providing the machines and Mr. Ingo Danner for pleasant and efficient collaboration during the experiment. Finally, thanks are due to Dr. Irina Kuzyakova for statistical consultation and to Prof. Dr. Stephan Peth for advice concerning the interpretation of the results.

6. References

Ala-Ilomäki, J., Högnäs, T., Lamminen, S., Sirén, M., 2011: Equipping a Conventional Wheeled Forwarder for Peatland Operations. Int. J. Forest Eng. 22(1): 7–13. https://doi.org/10.1080/14942119.2011.10702599

Ala-Ilomäki, J., Lindeman, H., Mola-Yudego, B., Prinz, R., Väätainen, K., Talbot, B., Routa, J., 2021: The effect of bogie track and forwarder design on rut formation in a peatland. Int. J. Forest Eng. 32(1): 12–19. https://doi.org/10.1080/14942119.2021.1935167

Allman, M., Jankovský, M., Messingerová, V., Allmanová, Z., 2017: Soil moisture content as a predictor of soil disturbance caused by wheeled forest harvesting machines on soils of the Western Carpathians. J. For. Res. 28(2): 283–289. https://doi.org/10.1007/s11676-016-0326-y

Amelung, W., Blume, H.P., Fleige, H., Horn, R., Kandeler, E., Kögel-Knabner, I., Kretzschmar, R., Stahr, K., Wilke, B.M., 2018: Scheffer/Schachtschabel Lehrbuch der Bodenkunde. 17. Auflage. Springer Spektrum, Berlin.

Ampoorter, E., Goris, R., Cornelis, W.M., Verheyen, K., 2007: Impact of mechanized logging on compaction status of sandy forest soils. For. Ecol. Manage. 241(1–3): 162–174. https://doi.org/10.1016/j.foreco.2007.01.019

Bachmann, J., Horn, R., Peth, S., 2014: Hartge/Horn: Einführung in die Bodenphysik. 4. Auflage. Schweizerbart, Stuttgart, 1–372.

Bates, D., Maechler, M., Bolker, B., Walker, S., 2015: Fitting Linear Mixed-Effects Models Using lme4. J. Stat. Softw. 67(1): 1–48. https://doi.org/10.18637/jss.v067.i01

Bygdén, G., Eliasson, L., Wästerlund, I., 2003: Rut depth, soil compaction and rolling resistance when using bogie tracks. J. Terramech. 40(3): 179–190. https://doi.org/10.1016/j.jterra.2003.12.001

Cambi, M., Certini, G., Neri, F., Marchi, E., 2015: The impact of heavy traffic on forest soils: A review. For. Ecol. Manage. 338: 124–138. http://dx.doi.org/10.1016/j.foreco.2014.11.022

Carter, M.R., 1990: Relative measures of soil bulk density to characterize compaction in tillage studies on fine sandy loams. Can. J. Soil Sci. 70(3): 425–433.

Cavalli, R., Amishev, D., 2019: Steep terrain forest operations – challenges, technology development, current implementation, and future opportunities. Int. J. Forest Eng. 30(3): 175–181. https://doi.org/10.1080/14942119.2019.1603030

DIN Deutsches Institut für Normung e.V., 2012: DIN 18127:2012-09, Soil, investigation and testing – Proctor-test.

DIN Deutsches Institut für Normung e.V., 2017: Geotechnical investigation and testing –Laboratory testing of soil – Part 4: Determination of particle size distribution (ISO 17892-4:2016); German version EN ISO 17892-4:2016

DIN Deutsches Institut für Normung e.V., 2020: DIN 4220:2020-11, Bodenkundliche Standortbeurteilung – Kennzeichnung, Klassifizierung und Ableitung von Bodenkennwerten (normative und nominale Skalierungen).

Durner, W., Iden, S., 2021: The improved integral suspension pressure method (ISP+) for precise particle size analysis of soil and sedimentary materials. Soil Tillage Res. 213: 105086. https://doi.org/10.1016/j.still.2021.105086

Ecoforst GmbH, 2018: T-Winch 10.1 Product brochure. Retrieved from https://www.ecoforst.at/ on 2021-01-14

Eliasson, L., 2005: Effects of forwarder tyre pressure on rut formation and soil compaction. Silva Fenn. 39(4): 549–557. https://doi.org/10.14214/sf.366

Eliasson, L., Wästerlund, I., 2007: Effects of slash reinforcement of strip roads on rutting and soil compaction on a moist fine-grained soil. For. Ecol. Manage. 252(1–3): 118–123. https://doi.org/10.1016/j.foreco.2007.06.037

Froehlich, H.A., 1978. Soil compaction from low ground-pressure, torsion-suspension logging vehicles on three forest soils. Research Paper 36, Forest Research Lab, Oregon State University.

Garren, A.M., Bolding, M.C., Aust, W.M., Moura, A.C., Barrett, S.M., 2019: Soil Disturbance Effects from Tethered Forwarding on Steep Slopes in Brazilian Eucalyptus Plantations. Forests 10(9): 721. https://doi.org/10.3390/f10090721

Gelin, O., Björheden, R., 2020: Concept evaluations of three novel forwarders for gentler forest operations. J. Terramech. 90: 49–57. https://doi.org/10.1016/j.jterra.2020.04.002

Haas, J., Hagge Ellhöft, K., Schack-Kirchner, H., Lang, F., 2016: Using photogrammetry to assess rutting caused by a forwarder – A comparison of different tires and bogie tracks. Soil Tillage Res. 163: 14–20. https://doi.org/10.1016/j.still.2016.04.008

HessenForst, 2018: Betriebsbuch Forstamt Hessisch Lichtenau (Forest inventory and planning documentation of the Hessen state forest service, Hessisch Lichtenau branch office).

Holzfeind, T., Kanzian, C., Stampfer, K., Holzleitner, F., 2019: Assessing Cable Tensile Forces and Machine Tilt of Winch-Assisted Forwarders on Steep Terrain under Real Working Conditions. Croat. J. For. Eng. 40(2): 281–296. https://doi.org/10.5552/crojfe.2019.621

Holzfeind, T., Visser, R., Chung, W., Holzleitner, F., Erber, G., 2020: Development and Benefits of Winch-Assist Harvesting. Curr. For. Rep. 6: 201–209. https://doi.org/10.1007/s40725-020-00121-8

Holzleitner, F., Kastner, M., Stampfer, K., Höller, N., Kanzian, C., 2018: Monitoring Cable Tensile Forces of Winch-Assist Harvester and Forwarder Operations in Steep Terrain. Forests 9(2): 53. https://doi.org/10.3390/f9020053

ISO International Organization for Standardization, 2022: ISO 19472-2:2022, Machinery for forestry – Winches – Part 2: Traction aid winches.

John Deere, 2019: G-Series Forwarders. Product brochure. Retrieved from https://www.deere.com/ on 2021-06-01.

Kuznetsova, A., Brockhoff, P.B., Christensen, R.H.B., 2017: lmerTest Package: Tests in Linear Mixed Effects Models. J. Stat. Softw. 82(13): 1–26. https://doi.org/10.18637/jss.v082.i13

Labelle, E.R., Jaeger, D., 2011: Soil Compaction Caused by Cut-to-Length Forest Operations and Possible Short-Term Natural Rehabilitation of Soil Density. Soil Sci. Soc. Am. J. 75(6): 2314–2329. https://doi.org/10.2136/sssaj2011.0109

Labelle, E.R., Jaeger, D., 2012: Quantifying the Use of Brush Mats in Reducing Forwarder Peak Loads and Surface Contact Pressures. Croat. J. For. Eng. 33(2): 249–274.

Labelle, E.R., Jaeger, D., 2019: Effects of Steel Flexible Tracks on Forwarder Peak Load Distribution: Results from a Prototype Load Test Platform. Croat. J. For. Eng. 40(1): 1–23.

Labelle, E.R., Jaeger, D., 2021: Influence of Saturated Organic Matter on the Accuracy of In-Situ Measurements Recorded with a Nuclear Moisture and Density Gauge. Croat. J. For. Eng. 42(2): 357–367. https://doi.org/10.5552/crojfe.2021.762

Labelle, E.R., Hansson, L., Högbom, L., Jourgholami, M., Laschi, A., 2022: Strategies to Mitigate the Effects of Soil Physical Disturbances Caused by Forest Machinery: a Comprehensive Review. Curr. For. Rep. 8: 20–37. https://doi.org/10.1007/s40725-021-00155-6

McKenzie, D.W., Richardson, B.Y., 1978: Feasibility study of self-contained tether cable system for operating equipment on slopes of 20–75%. J. Terramech. 15(3): 113–127. https://doi.org/10.1016/0022-4898(78)90015-0

McNabb, D.H., Startsev, A.D., Nguyen, H., 2001: Soil Wetness and Traffic Level Effects on Bulk Density and Air-Filled Porosity of Compacted Boreal Forest Soils. Soil Sci. Soc. Am. J. 65(4): 1238–1247. https://doi.org/10.2136/sssaj2001.6541238x

Mellgren, P.G., 1980: Terrain Classification for Canadian Forestry. Woodlands Section, Canadian Pulp and Paper Association, 1–13.

METER Group AG, 2021: PARIO Soil Particle Analyzer. Operating manual.

Mologni, O., Dyson, P., Amishev, D., Proto, A., Zimbalatti, G., Cavalli, R., Grigolato, S., 2018: Tensile Force Monitoring on Large Winch-Assist Forwarders Operating in British Columbia. Croat. J. For. Eng. 39(2): 193–204.

Naghdi, R., Solgi, A., Labelle, E.R., Nikooy, M., 2020: Combined effects of soil texture and machine operating trail gradient on changes in forest soil physical properties during ground-based skidding. Pedosphere 30(4): 508–516. https://doi.org/10.1016/S1002-0160(17)60428-4

R Core Team, 2021: R: A language and environment for statistical computing. R Foundation for Statistical Computing, Vienna, Austria. https://www.r-project.org/

Raghavan, G., McKyes, E., Chassé, M., 1977: Effect of wheel slip on soil compaction. J. Agr. Eng. Res. 22: 79–83.

Renius, K.T., 2020: Fundamentals of Tractor Design. Springer Nature Switzerland. https://doi.org/10.1007/978-3-030-32804-7

Ringdahl, O., Hellström, T., Wästerlund, I., Lindroos, O., 2012: Estimating wheel slip for a forest machine using RTK-DGPS. J. Terramech. 49(5): 271–279. https://doi.org/10.1016/j.jterra.2012.08.003

RStudio Team, 2021: RStudio: Integrated Development Environment for R. RStudio, PBC, Boston, MA. http://www.rstudio.com/

Salmivaara, A., Launiainen, S., Perttunen, J., Nevalainen, P., Pohjankukka, J., Ala-Ilomäki, J., Sirén, M., Laurén, A., Tuomine, S., Uusitalo, J., Pahikkala, T., Heikkonen, J., Finér L., 2020: Towards dynamic forest trafficability prediction using open spatial data, hydrological modelling and sensor technology. Forestry 93(5): 662–674. https://doi.org/10.1093/forestry/cpaa010

Schönauer, M., Holzfeind, T., Hoffmann, S., Holzleitner, F., Hinte, B., Jaeger, D., 2020: Effect of a traction-assist winch on wheel slippage and machine induced soil disturbance in flat terrain. Int. J. Forest Eng. 32(1): 1–11. https://doi.org/10.1080/14942119.2021.1832816

Sessions, J., Leshchinsky, B., Chung, W., Boston, K., Wimer, J., 2017: Theoretical Stability and Traction of Steep Slope Tethered Feller-Bunchers. For. Sci. 63(2): 192–200. http://dx.doi.org/10.5849/forsci.16-069

Starke, M., Derron, C., Heubaum, F., Ziesak, M., 2020: Rut Depth Evaluation of a Triple-Bogie System for Forwarders – Field Trials with TLS Data Support. Sustainability 12(16): 6412. https://doi.org/10.3390/su12166412

United States Deparmtent of Agriculture, 1987: USDA Textural Soil Classification. Study Guide, Soil Mechanics Level I.

Visser, R., Stampfer, K., 2015: Expanding Ground-based Harvesting onto Steep Terrain: A Review. Croat. J. For. Eng. 36(2): 321–331.

Wästerlund, I., 1989: Strength components in the forest floor restricting maximum tolerable machine forces. J. Terramech. 26(2): 177–182. https://doi.org/10.1016/0022-4898(89)90005-0

Wiberg, V., Servin, M., Nordfjell, T., 2021: Discrete element modelling of large soil deformations under heavy vehicles. J. Terramech. 93: 11–21. https://doi.org/10.1016/j.jterra.2020.10.002

Wickham, H., 2016: ggplot2: Elegant Graphics for Data Analysis. Springer-Verlag New York.

Yokohama Off-Highway Tires, 2021: Product description. Retrieved from https://yokohama-oht.com/ on 2021-06-01

Zhao, Y., Krzic, M., Bulmer, C.E., Schmidt, M.G., Simard, S.W., 2010: Relative bulk density as a measure of compaction and its influence on tree height. Can. J. Forest Res. 40(9): 1724–1734. https://doi.org/10.1139/X10-115

Authors' addresses:

Lorenz Breinig, PhD *
e-mail: lorenz.breinig@uni-goettingen.de
Bastian Hinte, PhD
e-mail: bastian.hinte@forst.thueringen.de
Marian Schönauer, PhD
e-mail: marian.schoenauer@mendelu.cz
Stephan Hoffmann, PhD
e-mail: stephan.hoffmann@nibio.no
Henrik Brokmeier, PhD
e-mail: henrik.brokmeier@uni-goettingen.de
Prof. Dirk Jaeger, PhD
e-mail: dirk.jaeger@uni-goettingen.de
University of Göttingen
Faculty of Forest Sciences and Forest Ecology
Department of Forest Work Science and Engineering
Büsgenweg 4
DE-37077 Göttingen
GERMANY

* Corresponding author

Received: August 01, 2023
Accepted: July 19, 2024